ELSEVIER

Microelectronics Journal 33 (2002) 479–486

Microelectronics Journal

www.elsevier.com/locate/mejo

Nonautonomous pulse-driven chaotic oscillator based on Chua's circuit

A.S. Elwakil*

Department of Electrical and Computer Engineering, Faculty of Engineering, University of Sharjah, P.O. Box 27272 Sharjah, United Arab Emirates

Received 30 May 2001; revised 22 October 2001; accepted 9 November 2001

Abstract

A novel nonautonomous chaotic oscillator based on the passive structure of Chua's circuit is proposed. Unlike most of the available members of this class of chaotic oscillators, the proposed circuit is driven by a periodic bipolar pulse-train rather than by sinusoidal excitation. This results in equilibrium points which have fixed positions in space. The circuit employs self feedback via a single comparator, which is the only nonlinear device involved. The output of this comparator is a chaotic bipolar pulse-train. A mathematical model which captures the behavior of the circuit is derived and experimental results are presented. Also, a version of the circuit with a practical realization of the driving pulse generator is considered and a variant structure with an alternatively excited node is discussed.

Keywords: Chaos; Oscillators; Relaxation oscillators; Nonautonomous oscillators

1. Introduction

Nonautonomous chaotic oscillators form a class of circuits which produce chaos while being driven (excited) by an external time-varying source. While there are many known autonomous chaotic oscillators (see Ref. [1] and the references therein), very few nonautonomous chaotic oscillators have been introduced in the literature [2–4] following some classical systems, which have been studied in detail [5–7]. The reason for such limited number might be the lack of any evidence that the statistical features (eigenvalues, Lyapunov exponents, etc.) of the chaos produced by nonautonomous oscillators possesses any unique property which is not possessed by the chaos produced from autonomous oscillators. Moreover, the performance of nonautonomous oscillators is greatly affected by the quality of the utilized driving force generator.

It can be seen from Refs. [2–7] that a sinusoidal excitation method has always been adopted in those nonautonomous oscillators which have been reported. This automatically implies that the equilibrium points of these driven systems are time varying. The amplitude and frequency of the sinusoid both contribute to the chaotic dynamics. In Ref. [8], the effect of sinusoidal excitation on Chua's circuit was studied. To the best of our knowledge, a nonautonomous chaotic oscillator where the driving force is a pulse-train, rather than a sinusoid, has not yet been proposed. Therefore, in this work we aim to present such an oscillator based on the third-order passive structure of Chua's circuit.

Since a bipolar pulse-train switches between two fixed amplitude levels, the corresponding equilibrium points of the circuit remain fixed in space and not time varying. In place of the classical Chua's diode nonlinear resistor [9], we utilize a single comparator as the only nonlinear device in the circuit. Note that a comparator has a nonlinear V_i–V_0 characteristic whereas Chua's diode has a nonlinear V_i–I_i characteristic. Therefore, self-feedback is employed from the comparator's output to the excited node.

One main advantage of the proposed chaotic oscillator is its suitability for interfacing with digital circuitry. The driving force can well be a periodic digital clock; the output of the comparator is a chaotic pulse-train compatible with the input levels to a following digital system.

In Section 2, a mathematical model capturing the dynamics of the proposed circuit is derived and its chaotic nature experimentally verified. In Section 3, we replace the driving pulse-train with a practical circuit realization in order to clarify the higher-dimensional nature of the circuit. Finally, in Section 4, a variant structure with excitation applied to an alternative node is discussed.

* Permanent address: The Reactor Department, Egyptian Nuclear Research Center, Cairo, Egypt. Tel.: +971-6-505-0978; fax: +971-6-558-5191.

E-mail addresses: elwakil@ee.ucd.ie (A.S. Elwakil), elwakil@sharjah.ac.ae (A.S. Elwakil).

0026-2692/02/$ - see front matter
PII: S0026-2692(01)00156-2

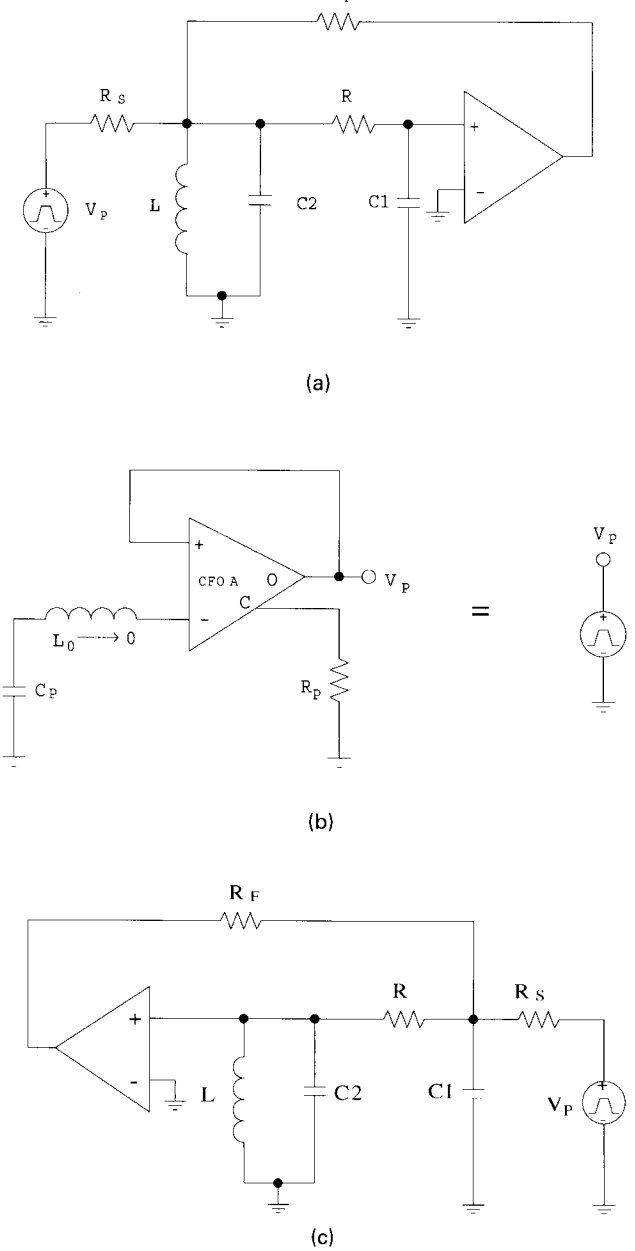

Fig. 1. Proposed pulse-driven nonautonomous chaotic oscillator: (a) circuit structure with excitation across C_2; (b) practical realization of the pulse-train generator; (c) alternative structure with excitation across C_1.

2. Proposed nonautonomous chaotic oscillator

Consider the circuit shown in Fig. 1(a) where the passive structure of Chua's circuit, composed of the LC_2 tank resonator, and the RC_1 low-pass filter section, can be clearly recognized. The output of a comparator, which is controlled via the voltage across C_1, is fed back to the excited node via resistor R_F. The driving force V_P is a pulse-train coupled via R_S to the same node. The output levels of both V_P and the comparator are bipolar and equal to $\pm V_{CC}$, where $\pm V_{CC}$ are the bias supplies for the comparator chip. The circuit in Fig. 1 is therefore described by:

$$L\dot{I}_L = V_{C2} \tag{1a}$$

$$C_2\dot{V}_{C2} = \frac{V_{C1}}{R} - \left(\frac{1}{R} + \frac{1}{R_S} + \frac{1}{R_F}\right)V_{C2} - I_L + \frac{V_P}{R_S} + \frac{V_N}{R_F} \tag{1b}$$

$$C_1\dot{V}_{C1} = \frac{V_{C2} - V_{C1}}{R} \tag{1c}$$

where V_N and V_P are the output voltages of the comparator and the driving pulse-train, expressed respectively as:

$$V_N = V_{CC}\,\mathrm{sgn}(V_{C1}) = \begin{cases} V_{CC} & V_{C1} \geq 0 \\ -V_{CC} & V_{C1} < 0 \end{cases} \tag{2a}$$

and

$$V_P = V_{CC}\,\mathrm{sgn}(\sin(\omega_P t)) \tag{2b}$$

Here, ω_P is the frequency of oscillation of the pulse-train.

By introducing the following dimensionless variable: $X = V_{C1}/V_{CC}$, $Y = V_{C2}/V_{CC}$, $Z = RI_L/V_{CC}$, $\tau = \omega_P t$, $\epsilon_c = C_1/C_2$, $\alpha_1 = L\omega_P/R$, $\alpha_2 = RC_2\omega_P$, $\beta_F = R/R_F$, and $\beta_S = R/R_S$ the previous set of equations transform into:

$$\begin{pmatrix} \epsilon_c\dot{X} \\ \dot{Y} \\ \dot{Z} \end{pmatrix} = \begin{pmatrix} -\frac{1}{\alpha_2} & \frac{1}{\alpha_2} & 0 \\ \frac{1}{\alpha_2} & -\frac{1+\beta_F+\beta_S}{\alpha_2} & -\frac{1}{\alpha_2} \\ 0 & \frac{1}{\alpha_1} & 0 \end{pmatrix} \begin{pmatrix} X \\ Y \\ Z \end{pmatrix} + \begin{pmatrix} 0 \\ \frac{a}{\alpha_2} \\ 0 \end{pmatrix} \tag{3}$$

Note that all the parameters (α_1, α_2, β_F, β_S) in the previous state transition matrix are constants which are independent of the state of the comparator output or the driving force. The only parameter in Eq. (3) which depends on these two outputs is a, which is a switching constant given by:

$$a = \begin{cases} \beta_F + \beta_S P(\tau) & X \geq 0 \\ -\beta_F + \beta_S P(\tau) & X < 0 \end{cases} \tag{4a}$$

and

$$P(\tau) = \mathrm{sgn}(\sin\tau) = \begin{cases} 1 & \sin\tau \geq 0 \\ -1 & \sin\tau < 0 \end{cases} \tag{4b}$$

Since a does not appear in the state transition matrix, it has no effect on the dynamics of the system at the equilibrium points. It is clear that this switching constant will only affect the position in space of the equilibrium points of the system, which are given by: $(x_0, y_0, z_0) = (0, 0, a)$. Using Eq. (4a) and (4b), it is seen that there are in general four equilibrium points; two located in the positive X half-space equal to $(0,0,\beta_F \pm \beta_S)$ and two located in the negative X half-space equal to $(0,0, -\beta_F \pm \beta_S)$. In the special case where $\beta_F = \beta_S = \beta$, two of these points coincide with the origin.

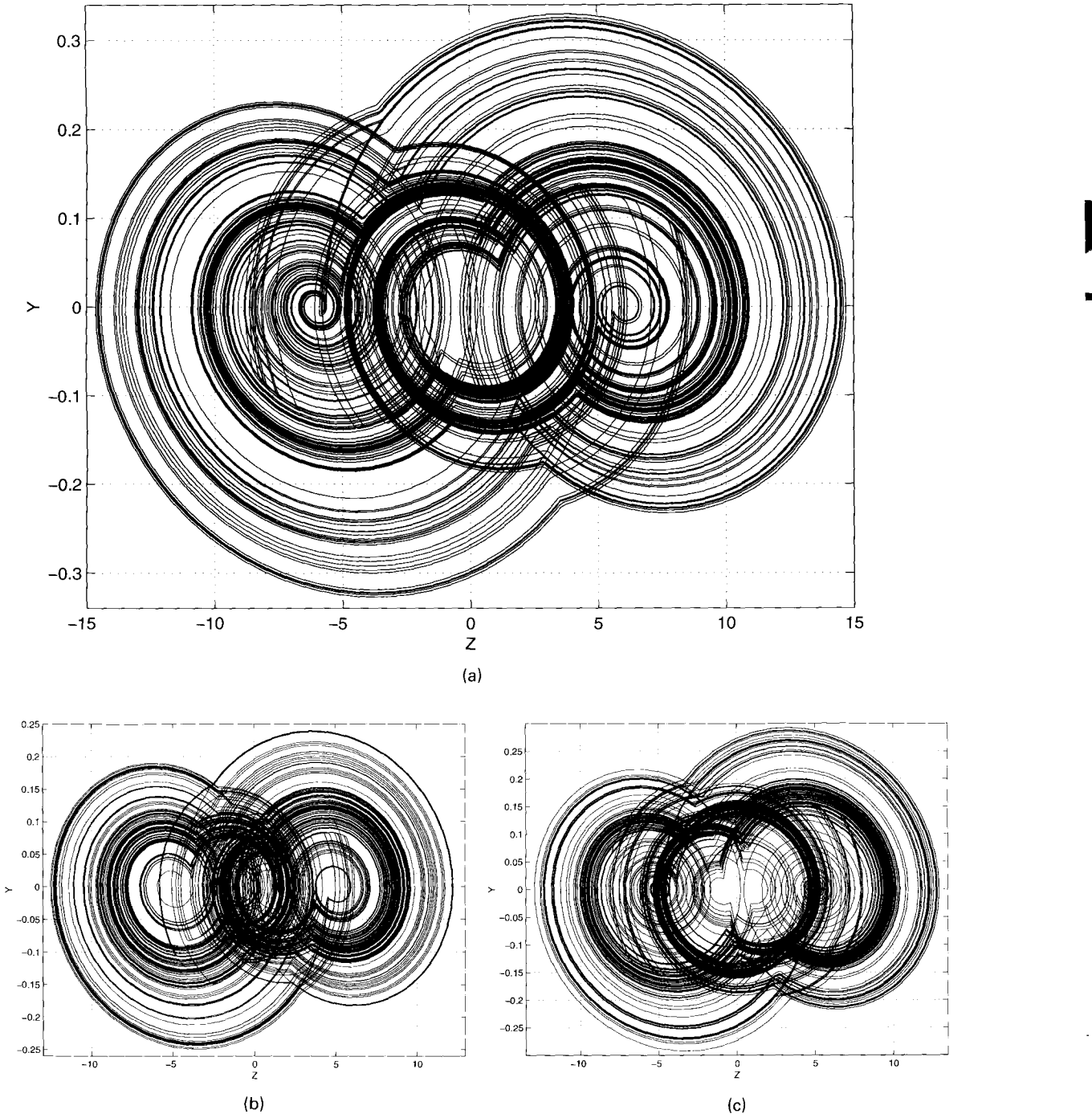

Fig. 2. Y–Z projection of the chaotic attractor obtained via numerical integration of Eq. (3) ($\alpha_1 = 0.05$, $\alpha_2 = 50$, $\epsilon_c = 0.2$): (a) $(\beta_F, \beta_S) = (3,3)$; (b) $(\beta_F, \beta_S) = (2,3)$ and (c) $(\beta_F, \beta_S) = (3,2)$.

Effectively, the system has three equilibrium points in this case; the origin and $(0,0, \pm 2\beta)$.

Numerical simulations of the previous model were performed using a Runge–Kutta algorithm with 0.001 step size and taking $\alpha_1 = 0.05$, $\alpha_2 = 50$, $\beta_F = \beta_S = 3$, $\tau = 0.1t$ and $\epsilon_c = 0.2$. In Fig. 2(a), the observed Y–Z projection of the chaotic attractor is shown. Note that the three equilibrium points in this case are the origin and $(0,0, \pm 6)$, which are clearly visible in the plot. In Fig. 2(b) and (c), the same projection is shown for the two cases: $(\beta_F, \beta_S) = (2,3)$ and (3,2), respectively. The equilibrium points in both cases are $(0,0, \pm 1)$ and $(0,0, \pm 5)$. Note that the condition $\beta_F > \beta_S$ implies that the two equilibrium points in the region $X > 0$ ($X < 0$) also lie in the region $Z > 0$ ($Z < 0$) while the condition $\beta_F < \beta_S$ implies alternating equilibrium points, i.e. when X switches from the

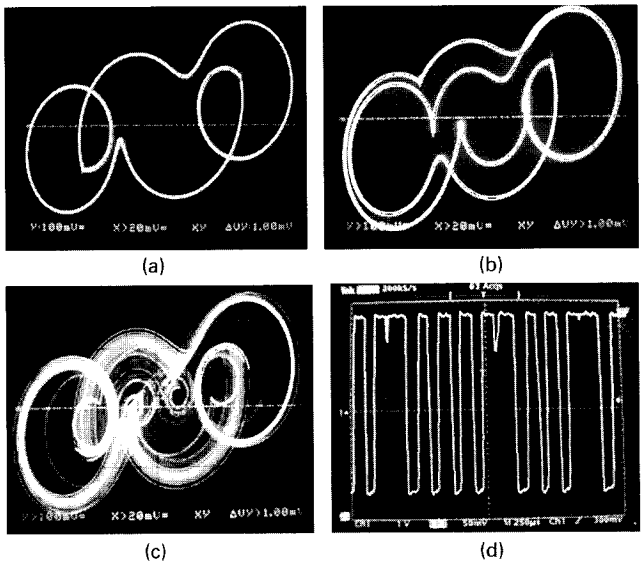

Fig. 3. Experimental V_{C1}–V_{C2} observations (X axis:20 mV/div, Y axis: 100 mV/div) (a) period-1 orbit (b) period-2 orbit (c) chaotic trajectory (d) sample chaotic pulse output waveform of the comparator (X axis: 250 μs/div, Y axis: 1 V/div).

positive to the negative half-space, Z will switch in the opposite direction.

An experimental setup of Fig. 1(a) was constructed taking $L = 1$ mH, $C_1 = 10$ nF, $C_2 = 100$ nF, $R = 5$ kΩ and using a general purpose TL082 op amp as the comparator. We have chosen to fix R_F at 1 kΩ and use a variable 5 kΩ resistor for R_S in order to tune the circuit dynamics. Noting that the resonant frequency of the LC_2 tank is approximately 16 kHz, the frequency of the driving pulse generator was scanned over the range of 1–20 kHz. The comparator was biased from ±5 V supplies and the pulse generator output was also fixed to ±5 V.

We have observed chaos in the range of frequencies 4–18 kHz. In Fig. 3(a), the period-one orbit observed at 5 kHz with $R_S = 1.528$ kΩ is shown. The period-two orbit in Fig. 3(b) is born at $R_S = 1.568$ kΩ whereas the chaotic trajectory in Fig. 3(c) corresponds to $R_S = 1.636$ kΩ. All projections represent the V_{C1}–V_{C2} (X–Y) phase plane since it is particularly difficult to measure the current in the inductor I_L (Z). In Fig. 3(d), a sample of the chaotic pulse-train generated at the comparator's output is shown. When the frequency of the pulse generator is increased to 15 kHz with $R_S = 1.907$ kΩ and $R = 7.6$ kΩ, we observe the double-scroll-like attractor shown in Fig. 4(a). The single-scroll, shown in Fig. 4(b), appears when R_S is increased to 1.952 kΩ. It is worth noting that the chaotic pulse-train generated at the comparator's output can be used in place of classical digital pseudo-random generators to feed a following digital circuit.

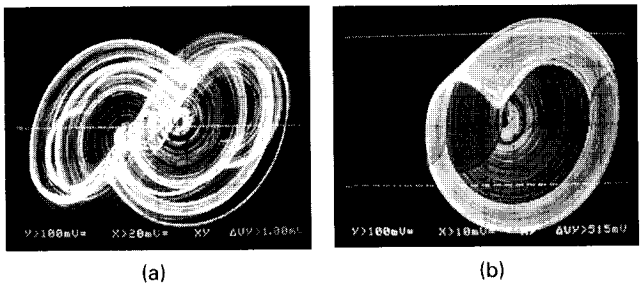

Fig. 4. Experimental observations at 15 kHz driving force frequency (X axis: 20 mV/div, Y axis: 100 mV/div), (a) double-scroll-like attractor, and (b) single-scroll attractor.

3. Practical pulse-train generator

It is well-known that practical pulse generators belong to the class of so-called relaxation oscillators, which involve dynamic hysteresis. It has been shown in Ref. [10] that hysteresis results from the interaction of a fundamentally nonlinear N-shaped (S-shaped) driving point characteristic with a parasitic capacitor (inductor). Therefore, relaxation oscillators are second-order systems which can be modeled accurately only when the underlying nonlinear characteristic and a suitable parasitic energy storage element are included [10,11]. In fact, any relaxation oscillator is a limit case condition of another sinusoidal oscillator when one of its energy storage elements becomes significantly small (compared to the rest of such elements in the circuit) such that it stimulates slow–fast dynamics, which are manifested as hysteresis [1].

Now, consider replacing the pulse generator in Fig. 1(a) by a possible practical realization, namely that shown in Fig. 1(b). One can then deduce that the exact order of the proposed nonautonomous chaotic oscillator is five. The circuit in Fig. 1(b) represents a novel relaxation oscillator with the minimum number of components based on a current feedback op amp (CFOA) [12,13]. The CFOA as it is connected together with resistor R_P form a current-controlled nonlinear resistor, the V_i–I_i characteristic of which is plotted in Fig. 5(a), for two different values of R_P. By placing a capacitor C_P in parallel with this resistor, hysteresis is stimulated and the parasitic inductor L_0 is necessary to model accurately this dynamical behavior. Thus, the following equations describe this oscillator:

$$C_P \dot{V}_{CP} = -I_{L0} \tag{5a}$$

$$L_0 \dot{I}_{L0} = V_{CP} - V_N \tag{5b}$$

where V_N is the voltage across the nonlinear resistor modeled in piecewise-linear form as:

$$V_N = \begin{cases} R^{\backslash}(I_{L0} - I_{sat}) - R_P I_{sat} & I_{L0} \geq I_{sat} \\ -R_P I_{L0} & -I_{sat} < I_{L0} < I_{sat} \\ R^{\backslash}(I_{L0} + I_{sat}) + R_P I_{sat} & I_{L0} \leq -I_{sat} \end{cases} \tag{6}$$

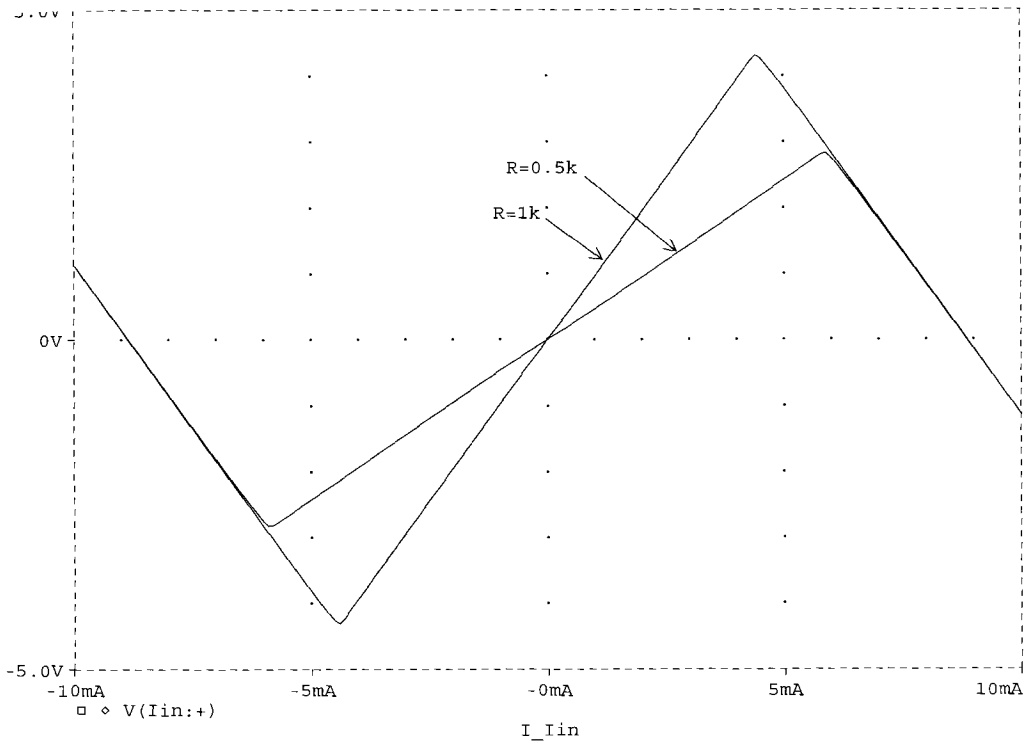

(a)

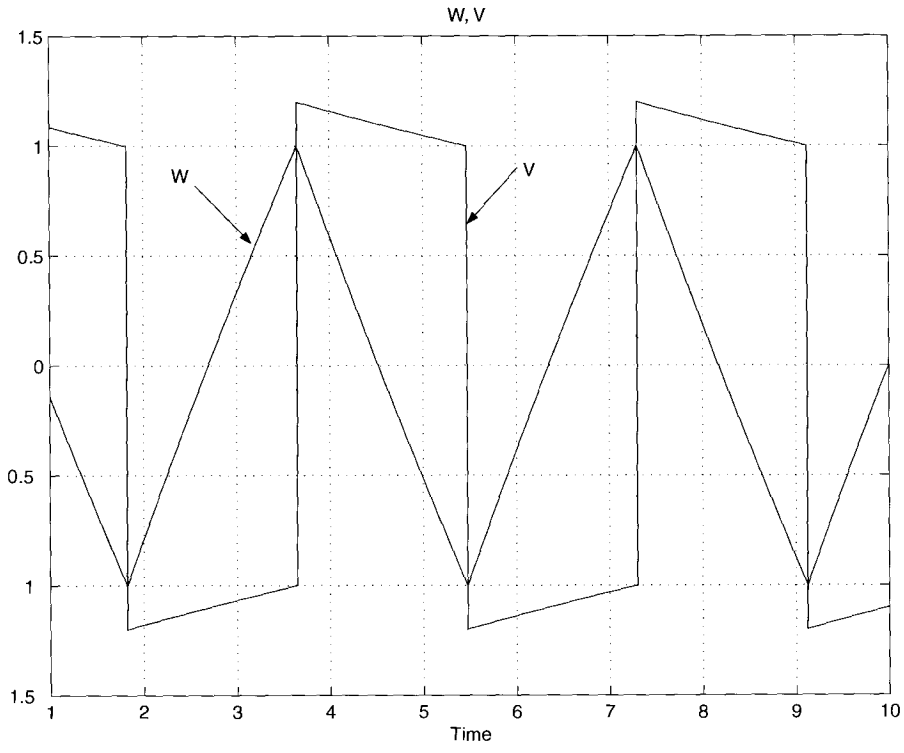

(b)

Fig. 5. (a) Characteristic of the CFOA S-shaped nonlinear resistor, (b) waveforms of the W and V state variables from the relaxation oscillator model ($\epsilon_P = 0.01$, $\beta_P = 10$).

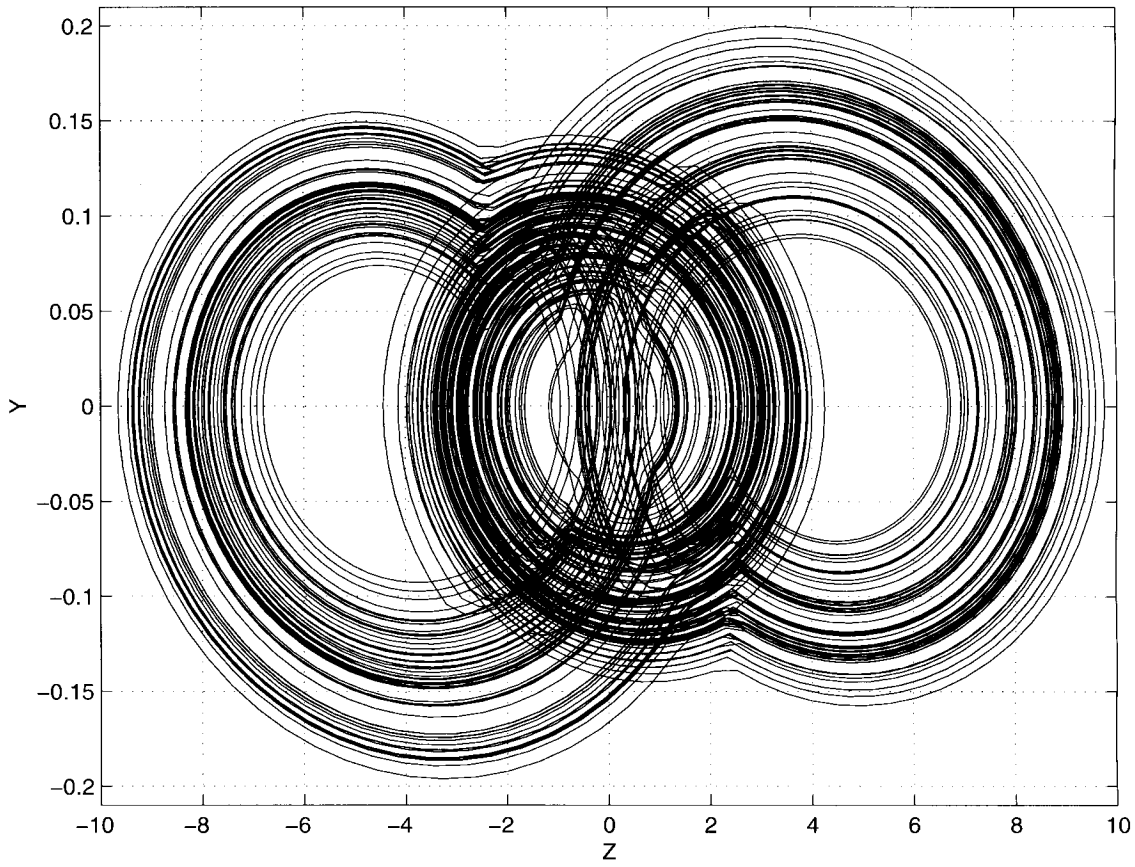

Fig. 6. Y–Z phase space projection from the fifth-order system equation Eq. (8) ($\alpha_1 = 0.003$, $\alpha_2 = 3$, $\beta_F = \beta_S = 3$, $\epsilon_c = 0.2$, $\epsilon_P = 0.01$, $\beta_P = 10$).

I_{sat} is the CFOA output saturation current and $R^{\backslash}$ is the value of the resistance in the outer segments of the nonlinear characteristics (see Fig. 5(a)).

By introducing the variables: $W = V_{CP}/V_{CC}$, $V = R_P I_{L0}/V_{CC} \equiv V_P$, $\tau = t/2C_P R_P$, $\epsilon_P = L_0/2C_P R_P^2$, $\beta_P = R^{\backslash}/R_P$ and $V_{CC} = R_P I_{sat}$, the previous model transforms into:

$$\begin{pmatrix} \dot{W} \\ \epsilon_P \dot{V} \end{pmatrix} = \begin{pmatrix} 0 & -2 \\ 1 & -b \end{pmatrix} \begin{pmatrix} W \\ V \end{pmatrix} + \begin{pmatrix} 0 \\ -c \end{pmatrix} \tag{7a}$$

and

$$(b,c) = \begin{cases} (\beta_P, -\beta_P - 1) & V \geq 1 \\ (-1, 0) & -1 < V < 1 \\ (\beta_P, \beta_P + 1) & V \leq -1 \end{cases} \tag{7b}$$

The time waveforms of the two state variables W and V are shown together in Fig. 5(b). Here, we have set $\epsilon_P = 0.01$ and $\beta_P = 10$.

By combining Eqs. (3), (7a) and (7b), the following full state-space representation of the nonautonomous chaotic oscillator can be deduced:

$$\begin{pmatrix} \epsilon_c \dot{X} \\ \dot{Y} \\ \dot{Z} \\ \dot{W} \\ \epsilon_P \dot{V} \end{pmatrix} = \begin{pmatrix} \frac{-1}{\alpha_2} & \frac{1}{\alpha_2} & 0 & 0 & 0 \\ \frac{1}{\alpha_2} & \frac{-(1+\beta_F+\beta_S)}{\alpha_2} & \frac{-1}{\alpha_2} & 0 & \frac{\beta_S}{\alpha_2} \\ 0 & \frac{1}{\alpha_1} & 0 & 0 & 0 \\ 0 & 0 & 0 & 0 & -2 \\ 0 & 0 & 0 & 1 & -b \end{pmatrix} \times \begin{pmatrix} X \\ Y \\ Z \\ W \\ V \end{pmatrix} + \begin{pmatrix} 0 \\ \frac{a}{\alpha_2} \\ 0 \\ 0 \\ -c \end{pmatrix} \tag{8}$$

where b and c are as given by Eq. (7b) while a is equal to β_F for $X \geq 0$ and equal to $-\beta_F$ for $X < 0$.

The Y–Z projection of the chaotic attractor from the above fifth-order system is shown in Fig. 6 for $\alpha_1 =$

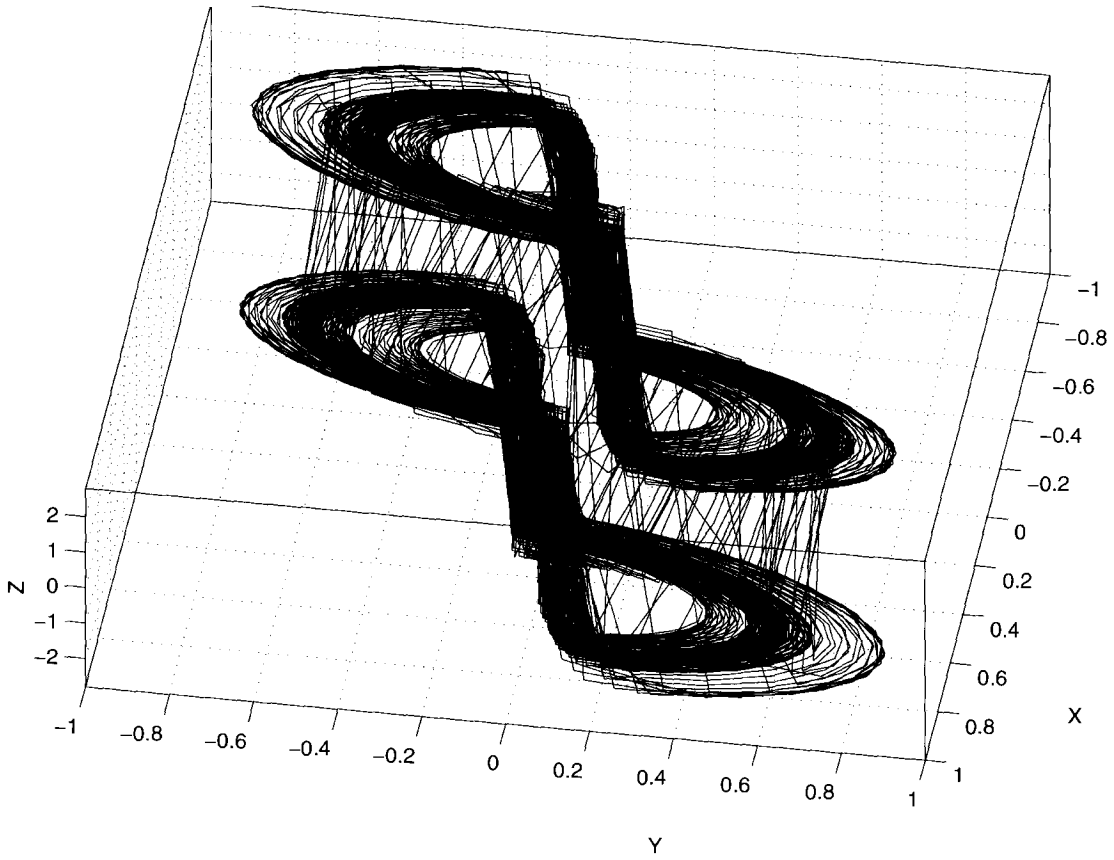

Fig. 7. X–Y–Z subspace chaotic attractor observed from the model of the alternatively excited circuit in Fig. 1(c).

0.003, $\alpha_2 = 3$, $\beta_F = \beta_S = 3$, $\epsilon_c = 0.2$, $\epsilon_P = 0.01$ and $\beta_P = 10$. The calculated eigenvalues corresponding to Fig. 6 are: $(-1.675, +2.042, +97.958, -1.162 \pm j10.449)$ in the region $-1 < V < 1$ and $(-1.675, -1.162 \pm j10.449, +0.075 \pm j14.142)$ in the other two regions of V. A single positive Lyapunov exponent equal to 0.205 was also calculated from the data corresponding to the Y time series.

Note that three of the eigenvalues, namely those with negative real part remain unchanged. These eigenvalues are the ones which can be calculated using Eq. (3). It is thus clear that the state transition matrix of Eq. (3) is insufficient to fully describe the dynamics of the oscillator at the equilibrium points. It is essential to expand the state-space of a nonautonomous chaotic oscillator into an appropriate higher-order dimension in order to accurately absorb the effect of the periodic driving force, which cannot be produced in practice by a zero-order system. Note that in reality, all nonautonomous chaotic oscillators involve two sources of nonlinearity, one responsible for folding the trajectories and the other embedded within the driving force and responsible for its stable limit cycle behavior.

4. Alternative configuration

The passive structure of Chua's circuit is a two-node structure. In Fig. 1(a), we have chosen to excite one of these nodes, namely the one across C_2. Here, we demonstrate the possibility of exciting the alternative node, i.e. the one across C_1. The circuit structure in this case is shown in Fig. 1(c) and is described by:

$$\begin{pmatrix} \epsilon_c \dot{X} \\ \dot{Y} \\ \dot{Z} \end{pmatrix} = \begin{pmatrix} 1 & -(1+\beta_F+\beta_S) & 0 \\ \dfrac{1}{\alpha_2} & -\dfrac{1}{\alpha_2} & -\dfrac{1}{\alpha_2} \\ 0 & \dfrac{1}{\alpha_1} & 0 \end{pmatrix} \begin{pmatrix} X \\ Y \\ Z \end{pmatrix} + \begin{pmatrix} a \\ 0 \\ 0 \end{pmatrix} \tag{9}$$

where a is as given by Eq. (4a) and (4b) with the switching condition dependent on Y instead of X.

Numerical integration of the previous equation was carried out after setting $\epsilon_c = 0.1$, $\alpha_1 = 0.07$, $\alpha_2 = 0.5$ and $\beta_F = \beta_S = 3$. For clarity, the observed projection of the chaotic attractor in the X–Y–Z subspace is shown in Fig. 7. The four equilibrium points of the system in this subspace are given by: $(x_0, y_0, z_0) = (-a, 0, -a)$ which are also fixed in space but are different from the ones offered by the previous node excitation. Following a procedure similar to that used to derive Eq. (8), Eq. (9) can be expanded into its governing five-dimensional space. From this expanded representation, the calculated eigenvalues corresponding

to Fig. 7 are: (2.185,0.291 $\pm j1.135$, $-0.5 \pm j1.323$) in the region $-1 < V < 1$ and (2.185,0.291 $\pm j1.135$,0.204,9.796) in the other two regions of V. A single positive Lyapunov exponent equal to 0.0089 was also calculated from the Y time series. It is similarly noticed here that the eigenvalues which can be calculated from Eq. (9) are the ones which remain unchanged in the expanded model.

5. Conclusion

A pulse-driven nonautonomous chaotic oscillator configuration with equilibrium points fixed in space was proposed. A basic advantage of this oscillator is its suitability for interconnection with digital circuits. We have clarified that the dynamics of this oscillator can accurately be modeled in a five-dimensional space when the driving force is replaced with its practical realization, essentially a second-order relaxation oscillator. It is clear that the number of equilibrium points in space are directly proportional to the sum of the possible voltage output levels of both the comparator and the driving pulse-train. Hence, if multi-level-logic is adopted, the number of equilibrium points can be increased. Excitation was investigated at the two nodes of the core passive structure, which is that of Chua's circuit.

Acknowledgements

Part of the equipment used in the experiments was donated by the Department of Electrical and Electronics Engineering at University College Dublin, Ireland. Many thanks for Mr A. A. Malik from Sharjah University for his lab assistance.

References

[1] A.S. Elwakil, M.P. Kennedy, Construction of classes of circuit-independent chaotic oscillators using passive-only nonlinear devices, IEEE Trans. Circuits Syst.-I 48 (2001) 289–307.
[2] A. Azzouz, R. Duhr, M. Hasler, Transition to chaos in a simple nonlinear circuit driven by a sinusoidal voltage source, IEEE Trans. Circuits Syst.-I 30 (1983) 913–914.
[3] K. Murali, M. Lakshmanan, L.O. Chua, The simplest dissipative nonautonomous chaotic circuit, IEEE Trans. Circuits Syst.-I 41 (1994) 462–463.
[4] J.G. Lacy, A simple piece-wise-linear nonautonomous circuit with chaotic behavior, Int. J. Bifurc. Chaos 6 (1996) 2097–2100.
[5] M.P. Kennedy, L.O. Chua, Van der Pol and chaos, IEEE Trans. Circuits Syst.-I 33 (1983) 974–980.
[6] S. Tanaka, T. Matsumoto, J. Noguchi, Multi-folding: alternative appearing of period-one attractors and chaotic attractors in a driven R–L-diode circuit, Phys. Lett. A 157 (1991) 37–42.
[7] S. Tanaka, J. Noguchi, S. Higuchi, T. Matsumoto, A repeated appearance of period-1 attractor in a driven R–L-diode circuit: experimental and theoretical bifurcation analysis, IEICE Trans. Fundam. E74 (1991) 1406–1413.
[8] K. Murali, M. Lakshmanan, Effect of sinusoidal excitation on Chua's circuit, IEEE Trans. Circuits Syst.-I 39 (1992) 264–270.
[9] M.P. Kennedy, Robust op amp realization of Chua's circuit, Frequenz 46 (1992) 66–80.
[10] M.P. Kennedy, L.O. Chua, Hysteresis in electronic circuits: a circuit theorist's perspective, Int. J. Circuit Theory Appl. 19 (1991) 471–515.
[11] A.S. Elwakil, Low-voltage relaxation oscillator, Electron. Lett. 36 (2000) 1256–1257.
[12] A.S. Elwakil, M.P. Kennedy, Improved implementation of Chua's chaotic oscillator using the current feedback op amp, IEEE Trans. Circuits Syst.-I 47 (2000) 76–79.
[13] A.S. Elwakil, M.P. Kennedy, Inductorless hyperchaos generator, Microelectron. J. 30 (1999) 739–743.